

Influence of excited states in high-order harmonic generation at intense mid-infrared field

Yan Fang(方言), Da-Wei Tian(田大纬), Yue Cao(曹玥), Xiao-Lei Hao(郝小雷), and Zheng Shu(舒正)
Citation: Chin. Phys. B, 2025, 34 (**10**): 103201. DOI: 10.1088/1674-1056/adda0d
http://cpb.iphy.ac.cn; http://iopscience.iop.org/cpb

What follows is a list of articles you may be interested in

Frequency shifts of high-order harmonics from ZnO crystals by chirped laser pulses

Yu Zhao(赵宇), Xiao-Jin Liu(刘晓瑾), Shuang Wang(王爽), Xiao-Xin Huo(霍晓鑫), Yun-He Xing(邢云鹤), and Jun Zhang(张军)
Chin. Phys. B, 2025, 34 (**3**): 033201. DOI: 10.1088/1674-1056/ada9dc

Role of excited states in helium-like ions on high-order harmonic generation

Jiang-Hua Luo(罗江华) and Jia-Jun Xiao(肖佳俊)
Chin. Phys. B, 2023, 32 (**11**): 113201. DOI: 10.1088/1674-1056/ace317

Phase-coherence dynamics of frequency-comb emission via high-order harmonic generation in few-cycle pulse trains

Chang-Tong Liang(梁畅通), Jing-Jing Zhang(张晶晶), and Peng-Cheng Li(李鹏程)
Chin. Phys. B, 2023, 32 (**3**): 033201. DOI: 10.1088/1674-1056/acac0f

Multiple collisions in crystal high-order harmonic generation

Dong Tang(唐栋) and Xue-Bin Bian(卞学滨)
Chin. Phys. B, 2022, 31 (**12**): 123202. DOI: 10.1088/1674-1056/ac6b2c

Probing subcycle spectral structures and dynamics of high-order harmonic generation in crystals

Long Lin(林龙), Tong-Gang Jia(贾铜钢), Zhi-Bin Wang(王志斌), and Peng-Cheng Li(李鹏程)
Chin. Phys. B, 2022, 31 (**9**): 093202. DOI: 10.1088/1674-1056/ac6943

SPECIAL TOPIC — Ultrafast physics in atomic, molecular and optical systems

Influence of excited states in high-order harmonic generation at intense mid-infrared field

Yan Fang(方言), Da-Wei Tian(田大纬), Yue Cao(曹玥), Xiao-Lei Hao(郝小雷), and Zheng Shu(舒正)†

State Key Laboratory of Quantum Optics Technologies and Devices, Institute of Theoretical Physics, Shanxi University, Taiyuan 030006, *China*

(Received 27 March 2025; revised manuscript received 12 May 2025; accepted manuscript online 19 May 2025)

We present a comprehensive study on the role of various excited states in high-order harmonic generation of hydrogen atoms driven by a long-wavelength (1500 nm) laser field. By numerically solving the time-dependent Schrödinger equation (TDSE) and performing a time-frequency analysis, we investigate the influence of individual excited states on the harmonic spectrum. Our results reveal that the 2s excited state primarily contributes to the enhancement of high-energy harmonic yields by facilitating long electron trajectories, while the 2p excited state predominantly suppresses harmonic yields in the lower-energy region (20th–50th orders) by altering the contributions of electron trajectories. Our results highlight the critical role of the excited states in the HHG process, even at longer laser wavelengths.

Keywords: high-order harmonic generation (HHG), strong-field physics, excited-state effect

PACS: 32.80.Rm, 42.65.Ky

DOI: 10.1088/1674-1056/adda0d **CSTR:** 32038.14.CPB.adda0d

1. Introduction

High-order harmonic generation (HHG), a fundamental process in strong-field physics and attosecond science, has emerged as a powerful spectroscopic technique for investigating ultrafast electron dynamics across atomic, molecular, and condensed matter systems.[1–10] The widely accepted semi-classical three-step model (ionization, acceleration, and recombination) provides a robust framework for interpreting HHG phenomena, successfully predicting characteristic spectral features such as the plateau region and cutoff energy.[11–13] However, recent experimental observations and theoretical studies have highlighted non-adiabatic quantum dynamics that the conventional model fails to fully account for, particularly in relation to the involvement of intermediate excited states during the recombination process.[14–16]

Recent studies have demonstrated that excited states influence the HHG process in various ways. These states provide additional ionization and recombination pathways, which can enhance harmonic generation in specific spectral regions or introduce new features into the harmonic spectrum.[17] For instance, bound-bound and bound-continuum transitions have been identified as contributing factors to low-order harmonics, while bound-continuum recombination dominates the high-order regime.[18–21]

Moreover, coherence between ground and excited states, as well as their population dynamics, plays a crucial role in shaping the HHG spectra.[22–24] The presence of excited states not only broadens the quantum path of ionization and recombination, but also significantly alters the harmonic spectral properties through energy level resonance effects. For example, in the coherent superposition state of the H_2^+ molecule, the interference between excited-state ionization and ground-state recombination leads to a significant enhancement of HHG, with efficiency several times higher than that of the pure ground-state path.[25] This enhancement stems from two mechanisms: (i) the lower ionization potential barrier in the excited state boosts the ionization probability, and (ii) the higher dipole moment associated with the excited state enhances the coupling of the electron to the ground state. Similarly, in pre-excited argon atoms, the high-order harmonics in the non-perturbative region are dominated by excited-state electrons undergoing a three-step process and coupling with both short or long trajectory interference effects to form a complex spectral structure.[26] The involvement of the first excited states can also influence the position of two-center interference in molecular HHG.[27] In more complex molecular systems, excited-state HHG exhibits multi-orbital participation. For instance, investigations of H_2^+ molecules revealed prominent two-center interference effects in HHG spectra under coherent superposition states, which can be utilized for precise determination of nuclear separation.[28] Similarly, studies on $CHBr_3$ demonstrated that the high-energy portion of harmonics originates from contributions of the HOMO-6 and HOMO-9 orbitals, deviating from the predictions of the conventional HOMO-based three-step model.[29] The excited-state effects in multi-electron systems present additional complexity, as exemplified by the ultrafast localization of bound electrons in H_3^+ molecules, which induces harmonic suppression phenomena

†Corresponding author. E-mail: zheng_shu@sxu.edu.cn

© 2025 Chinese Physical Society and IOP Publishing Ltd. All rights, including for text and data mining, AI training, and similar technologies, are reserved.

and provides a novel tool for investigating multi-electron dynamics.[30]

Recent experimental advances have also highlighted the role of excited states in HHG. Chini *et al.*[31] have identified a new regime of phase-matched below-threshold harmonic generation, which is associated with resonances between bound states. The influence of excited states in HHG has also been explored using the attosecond lighthouse technique, revealing novel spectral features that arise from ionization of excited states followed by recombination to the ground state.[32] Moreover, recent combined studies of coherent extreme ultraviolet free-induction decay and HHG have demonstrated that Rydberg-electron recapture predominantly occurs at the trailing edge of the driving laser field.[33]

In this paper, we provide a detailed analysis of the role of various excited states in HHG. By numerically solving the time-dependent Schrödinger equation (TDSE)[34,35] and employing time-frequency analysis, we demonstrate that different excited states influence specific regions of the HHG spectrum. Notably, the 2s excited state primarily affects the high-energy region, while the 2p excited state has a more pronounced impact on the lower-energy region. Furthermore, with the aid of time-frequency analysis, we find that the 2s excited state affects harmonic generation by influencing the long trajectories of the electron (including the second and third return trajectories), while the 2p excited state affects the contributions of electron trajectories in the lower-energy region of the high-harmonic spectrum.

2. Theoretical method

In this work, we employ three-dimensional (3D) models to describe the motion of an electron driven by a linearly polarized laser pulse, i.e., a z-polarized electric field. The TDSE is written as (throughout this paper, atomic units (a.u.) $e=\hbar=m_{\rm e}=1$ are used unless otherwise noted)

$$\mathrm{i}\partial_t\left|\Psi(t)\right\rangle=\hat{H}(t)\left|\Psi(t)\right\rangle, \tag{1}$$

with the Hamiltonian in velocity gauge

$$\hat{H}(t)=-\frac{1}{2}\nabla^2-\mathrm{i}\boldsymbol{A}(t)\cdot\nabla+U(r)-\mathrm{i}V_{\rm im}(r). \tag{2}$$

Here, $U(r)=-1/r$ is the Coulomb potential of the hydrogen atom. $A(t)$ denotes the vector potential. $V_{\rm im}$ is the imaginary potential employed to suppress unphysical reflections at the numerical boundary. The imaginary potential $V_{\rm im}$ is expressed as[36]

$$V_{\rm im}(r)=V_{\rm im,max}\left(\frac{r-R_{\rm im}}{W_{\rm im}}\right)^{16}\Theta(r-R_{\rm im}), \tag{3}$$

with $R_{\rm im}=R_{\rm I}+\alpha$, and $R_{\rm I}$ is the position of the flux-capturing surface for the time-dependent surface flux method.[37] $\alpha=E_0/\omega_0^2$ is the quiver amplitude of the electron under the laser field. The width of the imaginary potential $W_{\rm im}$ is set to 150 a.u.

The vector potential $\mathrm{A}(t)$ of the laser field is defined by a three-stage envelope over $n_{\rm c}=10$ optical cycles

$$A(t)=\begin{cases}\frac{E_0}{\omega_0}\sin^2\left(\frac{\omega_0 t}{8}\right)\sin(\omega_0 t), & t\le\frac{4\pi}{\omega_0},\\ \frac{E_0}{\omega_0}\sin(\omega_0 t), & \frac{4\pi}{\omega_0}<t<\frac{2\pi(n_{\rm c}-2)}{\omega_0},\\ \frac{E_0}{\omega_0}\sin^2\left(\frac{\omega_0 t-2\pi(n_{\rm c}-4)}{8}\right)\sin(\omega_0 t), & t\ge\frac{2\pi(n_{\rm c}-2)}{\omega_0},\end{cases} \tag{4}$$

where $E_0=0.0507$ a.u. is the peak field amplitude and $\omega_0=0.0507$ a.u. is the laser frequency.

To solve the TDSE, the wave function is expanded in terms of spherical harmonics[38]

$$\langle\boldsymbol{r}|\Psi(t)\rangle=\frac{1}{r}\sum_{\ell=0}^{N_\ell-1}\sum_{m=-\ell}^{\ell}\phi_{\ell m}(r,t)Y_{\ell m}(\theta,\phi), \tag{5}$$

where $\phi_{\ell m}(r,t)$ is the time-dependent radial function, and $Y_{\ell m}(\theta,\phi)$ is the spherical harmonic function. The radial wave function $\phi_{\ell m}(r,t)$ is discretized with units of $\Delta r=0.15$ a.u. In our simulation, the radial coordinate is restricted to $r_{\rm max}=555$ a.u. The maximum angular momentum quantum number $l_{\rm max}$ is set to 50. For the time evolution of Eq. (1), we take the Crank–Nicolson implicit method[39] with a time step of $\Delta t=0.0375$ a.u.

To obtain the bound eigenstates of the field-free Hamiltonian, the imaginary time propagation (ITP) is used in this paper.[40,41] The ITP method transforms the TDSE into an imaginary time framework, effectively converting quantum evolution into an energy minimization process. The time variable is substituted as $t\to-\mathrm{i}t$. The initial trial wavefunction can be assumed to be

$$\phi_0(\boldsymbol{r})=\sum c_n\phi_n, \tag{6}$$

where $\phi_n(\boldsymbol{r})$ corresponds to the eigenstates and $c_n=\langle\phi_n|\phi_0\rangle$. The time evolution of the initial wavefunction is expressed as

$$U(t)\phi_0(\boldsymbol{r})=\sum_{n=0}^{+\infty}c_n\,\mathrm{e}^{-\mathrm{i}t\varepsilon_n}\phi_n(\boldsymbol{r}), \tag{7}$$

where $U(t)=\exp(-\mathrm{i}\hat{H}(\boldsymbol{r})t)$ is the time evolution operator.

If the evolution time is sufficiently long, the high-energy components will decay exponentially, causing the wavefunction to converge to the ground state. In order to obtain the excited states, the trial wavefunction is imposed to be orthogonal to all of the lower energy eigenstates.

The expectation value of the acceleration is calculated as

$$\langle\ddot{d}(t)\rangle=-\left\langle\Psi(t)\left|\frac{\partial U(r)}{\partial z}\right|\Psi(t)\right\rangle-E(t), \tag{8}$$

and the HHG spectrum $\left|\langle\ddot{d}_\Omega\rangle\right|^2$ is calculated as

$$\langle\ddot{d}_\Omega\rangle=-\int_0^\infty W(t)\langle\ddot{d}(t)\rangle\,\mathrm{e}^{-\mathrm{i}\Omega t}\,\mathrm{d}t. \tag{9}$$

The window function $W(t)$ is selected as a Bartlett window. It is written as follows:[42]

$$W(t)=\begin{cases}\frac{2t}{N-1}, & 0\le t\le\frac{N-1}{2},\\ 2-\frac{2t}{N-1}, & \frac{N-1}{2}\le t\le N-1,\\ 0, & \text{others},\end{cases} \tag{10}$$

where N denotes the total number of points in the window length.

The populations of excited states are calculated through projecting the total wave function into the eigenstates of the hydrogen atom as follows:

$$|c_k(t)|^2=\left|\int_{-\infty}^{\infty}\phi_k^*(\boldsymbol{r})\Psi(\boldsymbol{r},t)\mathrm{d}\boldsymbol{r}\right|^2. \tag{11}$$

In order to exclude the contributions of excited states to HHG, the wave function $\Psi(\boldsymbol{r},t)$ in Eq. (1) is replaced by the modified wave function $\Psi'(\boldsymbol{r},t)=\Psi(\boldsymbol{r},t)-\sum_k c_k(t)\phi_k(\boldsymbol{r})$ at each time step. For example, to exclude the contribution of the 2s excited state, we first compute the projection coefficient

$$c_{2s}(t)=\int_{-\infty}^{\infty}\phi_{2s}^*(\boldsymbol{r})\Psi(\boldsymbol{r},t)\mathrm{d}\boldsymbol{r}. \tag{12}$$

Next, the time-dependent wave function of Eq. (1) is replaced by a new wave function given by

$$\Psi'(\boldsymbol{r},t)=\Psi(\boldsymbol{r},t)-c_{2s}(t)\phi_{2s}(\boldsymbol{r}). \tag{13}$$

3. Results and discussion

Figure 1 shows the populations of different excited states under a laser intensity of 0.9×10^{14} W/cm^2 at 1500 nm. The dashed line in Fig. 1 represents the oscillating laser field. It is evident that the 2p excited state exhibits the highest population, followed closely by the 2s and 3p excited states, which contribute at nearly the same level. Additionally, the 3s and 4s excited states show moderate populations, while the contributions from other excited states are minimal and can be considered negligible in the present analysis. Consequently, our subsequent discussion will focus on the influence of the 2s, 3s, 4s, 2p, and 3p excited states on HHG. For clarity, we categorize these excited states into two groups: s-type excited states (2s, 3s, 4s) and p-type excited states (2p, 3p).

Figure 2 illustrates the high-harmonic spectra of a hydrogen atom subjected to an intense laser field at a wavelength of 1500 nm, with a laser intensity of 0.9×10^{14} W/cm^2. The black squares in Fig. 2 represent the high-harmonic spectrum calculated with contributions from all excited states included. In Fig. 2(a), the red dots denote the high-harmonic spectrum obtained after excluding the contributions from the s-type excited states. It is evident that the exclusion of these states results in a significant decrease in harmonic yields in the spectral region above the 50th order, indicating that s-type excited states play a crucial role in enhancing high-energy harmonic yields.

Similarly, Fig. 2(b) presents the high-harmonic spectrum after excluding the contributions of the 2p and 3p excited states. A comparison with the spectrum that includes all excited states reveals a significant enhancement in harmonic yields within the lower-energy region (20th–50th orders) when the 2p and 3p states are excluded. This observation suggests that p-type excited states tend to suppress harmonic yields in this energy range. These findings demonstrate that different types of excited states exert distinct influences on the HHG process.

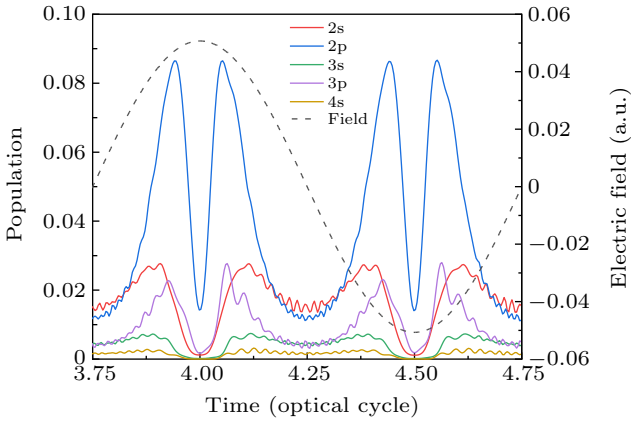


Fig. 1. Populations of various excited states of hydrogen under a laser intensity of 0.9×10^{14} W/cm^2 at 1500 nm. The dashed line indicates the oscillating laser field.

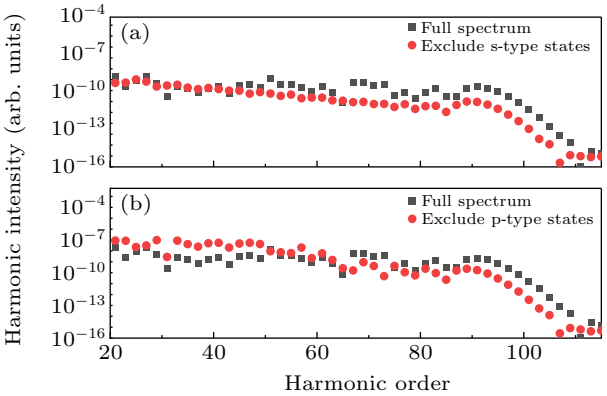


Fig. 2. High-harmonic spectra of a hydrogen atom subjected to an intense laser field at 1500 nm with a laser intensity of 0.9×10^{14} W/cm^2. Black squares represent the spectrum including all excited states. (a) Red dots show the spectrum after excluding s-type excited states. (b) Red dots show the spectrum after excluding p-type excited states.

To further investigate the impact of various excited states on HHG, we compute the high-harmonic spectra by sequentially removing the contributions from the 2s, 3s, 2p, and 3p excited states. Figures 3(a) and 3(b) display the harmonic spectra obtained after excluding the 2s and 3s excited states, respectively. In both cases, a suppression of harmonic yields in the high-energy region (above the 50th order) can be observed. However, the exclusion of the 2s state (Fig. 3(a)) re-

sults in a more pronounced reduction in harmonic yields relative to the full-spectrum result, while the suppression effect is less pronounced when the 3s state is excluded. Figures 3(c) and 3(d) present the harmonic spectra obtained after excluding the 2p and 3p excited states, respectively. In Fig. 3(c), the removal of the 2p state leads to a notable enhancement of harmonic yields in the lower-energy region (20th–50th orders). In contrast, excluding the 3p state (Fig. 3(d)) leads to only a marginal increase in harmonic yields within the same energy range. Therefore, as shown in Fig. 2, the primary differences between the full spectrum and the high-harmonic spectra obtained after excluding specific excited states are predominantly attributed to the contributions of the 2s and 2p excited states.

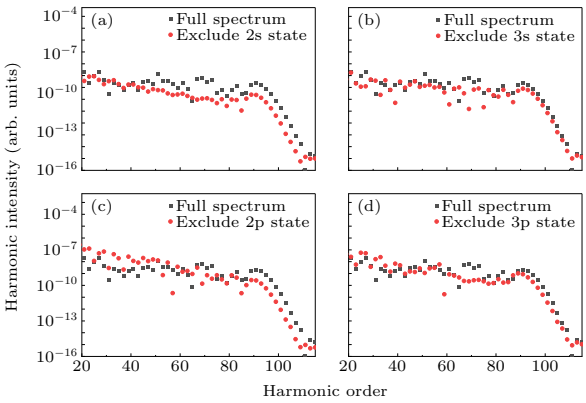


Fig. 3. High-harmonic spectra of a hydrogen atom subjected to an intense laser field at 1500 nm with a laser intensity of 0.9×10^{14} W/cm^2. Black squares represent the spectrum including all excited states. Panels (a)–(d) correspond to spectra after excluding the 2s, 3s, 2p, and 3p states, respectively.

To gain deeper insight into the physical mechanisms underlying the enhancement of high-energy harmonic yields due to the 2s excited state and the suppression of low-energy harmonic yields by the 2p excited state, we perform a time-frequency analysis using the wavelet transform of the induced dipole acceleration. The time profiles of harmonics are obtained via a Gabor transform[43] of the time-dependent dipole acceleration

$$\ddot{d}_{\rm G}(\omega,t)=\int_{-\infty}^{\infty}\exp(-{\rm i}\omega t')\exp\left(-\frac{(t'-t)^2}{2\sigma_0^2}\right)\ddot{d}(t')\,{\rm d}t', \quad (14)$$

where σ_0 is the width of the Gaussian time window. In the frequency domain, the width σ_0 in Eq. (14) corresponds to a Gaussian frequency filter with a spectral width of $10\omega_0$.

Figure 4(a) presents a representative modulus of the time-frequency profile including contributions from all excited states. This profile exhibits a well-defined curved structure in the first half of the optical cycle, repeating every half cycle, corresponding to short and long electron trajectories. In the second half of the cycle, additional complex structures emerge beneath the curved profile, associated with the second and third return trajectories. The black lines in Fig. 4(a) represent the classical electron trajectories from the three-step model.[12] It is evident that the second and third return trajectories are clearly reproduced by the time-frequency analysis.

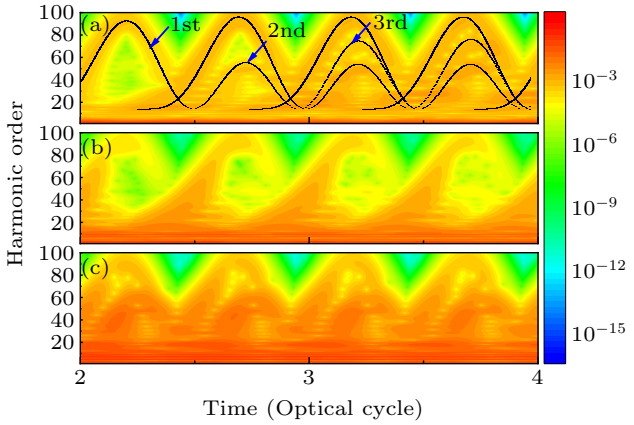


Fig. 4. Time-frequency analysis of the harmonic spectra shown in Fig. 2. (a) All excited states included. Black lines represent classical electron return trajectories from the three-step model. (b) Spectrum after excluding s-type excited states. (c) Spectrum after excluding p-type excited states.

Figure 4(b) shows the time-frequency distribution after excluding the s-type excited states. A comparison with Fig. 4(a) indicates that only the first return short trajectories remain. Figure 4(c) displays the time-frequency distribution after excluding the p-type excited states. In contrast to the s-type exclusion, both the first and second return trajectories remain. Notably, the harmonic emission intensities associated with these trajectories show an enhancement in the 20th–50th order region, which is consistent with Fig. 2(b).

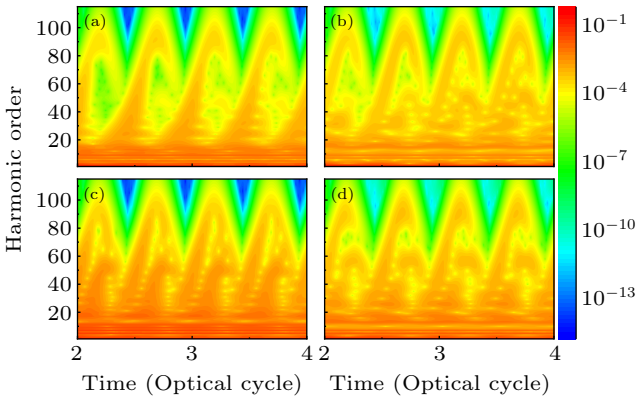


Fig. 5. Time-frequency analysis of the harmonic spectra shown in Fig. 3. Panels (a)–(d) correspond to spectra after excluding the 2s, 3s, 2p, and 3p states, respectively.

Figure 5 further presents the time-frequency distributions after separately excluding the 2s, 3s, 2p, and 3p excited states. The profile in Fig. 5(a) (2s excluded) closely resembles Fig. 4(b), where only the first return trajectory is preserved. In Fig. 5(b) (3s excluded), the second and third return trajectories remain visible but are significantly weaker than in Fig. 4(a). Excluding the 2p state (Fig. 5(c)) preserves both the first and second return trajectories while moderately enhancing harmonic yields within the 20th–50th order range, similar

to the p-type exclusion in Fig. 4(c). Finally, Fig. 5(d) (3p excluded) exhibits only a marginally weaker enhancement in the same low-energy region compared with the 2p-excluded case.

The analysis of the time-frequency results reveals that the 2s excited state plays a crucial role in facilitating the generation of long electron trajectories, whereas the 2p excited state primarily influences the relative contributions of different electron trajectories in the HHG process. Electrons following long trajectories experience extended transit times in the laser field, leading to a stronger spreading of their wave packets. The time-independent wave function of the 2s state is symmetrically distributed, while that of the 2p state is predominantly aligned along the polarization axis. As a result, the recombination amplitude for the 2s state is larger than that for the 2p state in long quantum trajectories (including the second and third returns). To verify this, we compare the relative contributions of the 2s and 2p states to the HHG process. The high-harmonic spectra are calculated by initializing the system in either the 2s or 2p state, with other bound states excluded using the projection method described in the theoretical section. Figure 6 shows the spectra for the 2s state (black line) and the 2p state (red line). The harmonic intensity from the 2s state is consistently higher than that from the 2p state in the order range of 20–80. Furthermore, for long-trajectory electrons, higher return energies correspond to shorter transit times, reducing the diffusion of the wave packet. Consequently, the 2s state has a more pronounced influence in the high-energy region.

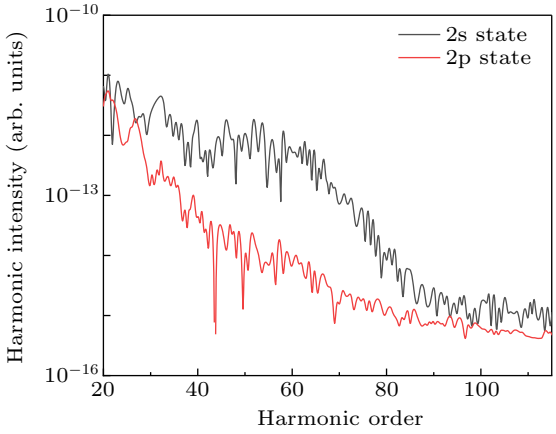


Fig. 6. High-harmonic spectra initiated from the 2s and 2p excited states at a laser intensity of 0.9×10^{14} W/cm^2 and wavelength of 1500 nm. Black line: spectrum starting from the 2s state with other bound states excluded. Red line: spectrum starting from the 2p state with other bound states excluded.

Figure 7 compares the population of the 2s state in two cases: with (black line) and without (red line) the inclusion of the 2p state. A reduction in the 2s population is observed when the 2p state is excluded, indicating that the absence of the 2p state increases the ionization probability of the 2s state. Moreover, lower-order harmonics generated via long trajectories correspond to ionization times closer to the peak of the laser field, where ionization probability is enhanced. This demonstrates that the 2p state plays a more significant role in shaping the low-energy region of the HHG spectrum.

These findings not only provide valuable insight into the distinct roles of the 2s and 2p excited states in HHG dynamics but also suggest strategies for controlling harmonic generation via the selective manipulation of excited states. Such understanding could guide the development of experimental techniques for optimizing HHG yields in practical applications.

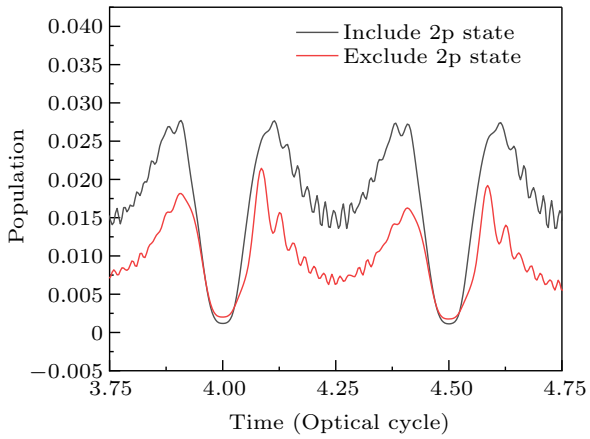


Fig. 7. Population of the 2s excited state. Black line: with the 2p state included. Red line: with the 2p state excluded.

4. Conclusion

In summary, we have presented a comprehensive analysis of the influence of various excited states on HHG driven by long-wavelength laser fields. To elucidate these effects, we employed a numerical approach by solving the TDSE and performing a time-frequency analysis of the harmonic spectra. Our results demonstrate that different excited states affect distinct regions of the HHG spectrum. The 2s state, owing to its symmetric wave function, predominantly enhances the high-energy region of the spectrum, particularly through contributions from long-trajectory electrons. In contrast, the 2p state, aligned mainly along the polarization axis, plays a key role in shaping the low-energy region by modulating ionization probabilities and altering contributions from lower harmonic orders. These findings not only advance the fundamental understanding of the interplay between excited states and HHG but also offer valuable insights into excited-state electron dynamics in long-wavelength laser fields, which may inform future strategies for optimizing harmonic generation.

Acknowledgment

This work was supported by the Scientific and Technological Innovation Programs of Higher Education Institutions in Shanxi.

References

[1] Eckle P, Pfeiffer A, Cirelli C, Staudte A, Dorner R, Muller H, Buttiker M and Keller U 2008 *Science* **322** 1525

[2] Schultze M, Fiess M, Karpowicz N, Gagnon J, Korbman M, Hofstetter M, Neppl S, Cavalieri A L, Komninos Y and Mercouris T 2010 *Science* **328** 1658

[3] Taylor D J and Paterson M J 2012 *Chem. Phys.* **408** 1

[4] Ott C, Kaldun A, Raith P, Meyer K, Laux M, Evers J, Keitel C H, Greene C H and Pfeifer T 2013 *Science* **340** 716

[5] Calegari F, Ayuso D, Trabattoni A, Belshaw L, De Camillis S, Anumula S, Frassetto F, Poletto L, Palacios A and Decleva P 2014 *Science* **346** 336

[6] Huppert M, Jordan I, Baykusheva D, Von Conta A and Wörner H J 2016 *Phys. Rev. Lett.* **117** 093001

[7] Teratani T, Mikami Y, Nakamoto N, Suzuki T, Harada Y, Okabayashi K, Hagihara Y, Taniki N, Kohno K and Shibata S 2020 *Nature* **585** 591

[8] Zhou S S, Yang Y J, Yang Y, Suo M Y, Li D Y, Qiao Y, Yuan H Y, Lan W D and Hu M H 2023 *Chin. Phys. B* **32** 013201

[9] Zhai C Y, Wu Y M, Qin L L, Li X, Shi L K, Zhang K, Kang S J, Li Z F, Li Y B, Tang Q B and Yu B H 2023 *Chin. Phys. B* **32** 073301

[10] Qiao Y, Chen J Q, Zhou S S, Chen J G, Jiang S C and Yang Y J 2024 *Chin. Phys. Lett.* **41** 014205

[11] Ferray M, L'Huillier A, Li X, Lompre L, Mainfray G and Manus C 1988 *J. Phys. B: At. Mol. Opt. Phys.* **21** L31

[12] Corkum P B 1993 *Phys. Rev. Lett.* **71** 1994

[13] Lewenstein M, Balcou P, Ivanov M Y, L'huillier A and Corkum P B 1994 *Phys. Rev. A* **49** 2117

[14] Lein M, Hay N, Velotta R, Marangos J P and Knight P L 2002 *Phys. Rev. Lett.* **88** 183903

[15] Vozzi C, Calegari F, Benedetti E, Caumes J P, Sansone G, Stagira S, Nisoli M, Torres R, Heesel E, Kajumba N, Marangos J P, Altucci C and Velotta R 2005 *Phys. Rev. Lett.* **95** 153902

[16] Shiner A D, Schmidt B E, Trallero-Herrero C, Wörner H J, Patchkovskii S, Corkum P B, Kieffer J C, Légaré F and Villeneuve D M 2011 *Nat. Phys.* **7** 464

[17] Figueira de Morisson Faria C, Dörr M and Sandner W 1998 *Phys. Rev. A* **58** 2990

[18] Carrera J J, Tong X M and Chu S I 2006 *Phys. Rev. A* **74** 023404

[19] Milošević D B 2006 *J. Opt. Soc. Am. B* **23** 308

[20] Kraus P M, Zhang S B, Gijsbertsen A, Lucchese R R, Rohringer N and Wörner H J 2013 *Phys. Rev. Lett.* **111** 243005

[21] Baykusheva D, Kraus P M, Zhang S B, Rohringer N and Wörner H J 2014 *Faraday Discuss.* **171** 113

[22] Telnov D A and Chu S I 2007 *Phys. Rev. A* **76** 043412

[23] Miller M R, Jaroń-Becker A and Becker A 2016 *Phys. Rev. A* **93** 013406

[24] Jiang S C and Dorfman K 2020 *Proc. Natl. Acad. Sci. USA* **117** 9776

[25] Phan A L and Le D N 2021 *Eur. Phys. J. B* **94** 165

[26] Li G H, Xie H Q, Li Z T, Yao J P, Chu W and Cheng Y 2017 *High Power Laser Sci. Eng.* **5** 26

[27] Chen Y J, Liu J and Hu B 2009 *Phys. Rev. A* **79** 033405

[28] Phan N L 2020 *Commun. Phys.* **30** 99

[29] Morassut C, Ravindran A, Ciavardini A, Luppi E, De Ninno G and Coccia E 2024 *J. Phys. Chem. A* **128** 2015

[30] Hu C X and He F 2024 *Phys. Rev. A* **109** 033113

[31] Chini M, Wang X W, Cheng Y, Wang H, Wu Y, Cunningham E, Li P C, Heslar J, Telnov D A, Chu S I and Chang Z H 2014 *Nat. Photonics* **8** 437

[32] Beaulieu S, Camp S, Descamps D, Comby A, Wanie V, Petit S, Légaré F, Schafer K J, Gaarde M B and Catoire F 2016 *Phys. Rev. Lett.* **117** 203001

[33] Peng S N, Chen Y D, Yang L, Fan G Y, Xie X H, He F and Tao Z S 2025 *Phys. Rev. Lett.* **134** 123203

[34] Kulander K C and Shore B W 1989 *Phys. Rev. Lett.* **62** 524

[35] Krause J L, Schafer K J and Kulander K C 1992 *Phys. Rev. Lett.* **68** 3535

[36] Gu B and Garashchuk S 2015 *AIP Conf. Proc.* **1702** 090014

[37] Tao L and Scrinzi A 2012 *New J. Phys.* **14** 013021

[38] Bauer D and Koval P 2006 *Comput. Phys. Commun.* **174** 396

[39] Crank J and Nicolson P 1947 *Math. Proc. Camb. Philos. Soc.* **43** 50

[40] Lehtovaara L, Toivanen J and Eloranta J 2007 *J. Comput. Phys.* **221** 148

[41] Trail J R 2008 *Phys. Rev. E* **77** 016703

[42] Bartlett M S 1950 *Biometrika* **37** 1

[43] Yuan K J and Bandrauk A D 2009 *Phys. Rev. A* **80** 053404